

# High-Density EMI Filter Design for DC-Fed Motor Drives

Yoann Maillet, Rixin Lai, *Member, IEEE*, Shuo Wang, *Senior Member, IEEE*, Fei (Fred) Wang, *Fellow, IEEE*, Rolando Burgos, *Member, IEEE*, and Dushan Boroyevich, *Fellow, IEEE*

**Abstract**—This paper presents strategies to reduce both differential-mode (DM) and common-mode (CM) noise using a passive filter in a dc-fed motor drive. The paper concentrates on the type of grounding and the components to optimize filter size and performance. Grounding schemes, material comparison between ferrite and nanocrystalline cores, and a new integrated filter structure are presented. The integrated structure maximizes the core window area and increases the leakage inductance by integrating both CM and DM inductances onto one core. Small-signal and large-signal experiments validate the structure, showing it to have reduced filter size and good filtering performance when compared with standard filters at both low and high frequencies.

**Index Terms**—Common mode (CM), differential mode (DM), electromagnetic interference (EMI), EMI filter, grounding, integrated filter.

## I. INTRODUCTION

ELECTROMAGNETIC interference (EMI) is one of the major design challenges in motor drive systems, especially in applications where stringent standards need to be followed. EMI noise is usually defined as common-mode (CM) and differential-mode (DM) noise. CM noise is defined as the noise flowing between the power circuit and the ground, while DM noise is defined as the current following the same path as the power delivery. Even though EMI standards only restrict the total noise, the noise is usually separated into CM and DM noise with a noise separator [1]. An understanding of the propagation of the noise facilitates filter design, since each filter mode can be considered separately.

Manuscript received May 30, 2009; revised August 1, 2009 and October 18, 2009. Current version published May 7, 2010. This work was supported by SAFRAN Group, by the National Science Foundation (NSF) under NSF Award Number EEC-9731677 and by the Center for Power Electronics Systems (CPES) Industry Partnership Program. Recommended for publication by Associate Editor P. Tenti.

Y. Maillet is with the Conver Team, Inc., Pittsburg, PA 15238 USA (e-mail: yoayo@vt.edu).

R. Lai is with the GE Global Research Center, Niskayuna, NY 12309 USA (e-mail: lairixin@vt.edu).

S. Wang is with the Electrical Power Systems, GE Aviation Systems, Vandalia, OH 45377-3062 USA (e-mail: shuowang@ieee.org).

F. (Fred) Wang is with The University of Tennessee, Knoxville, TN 37996 USA, and also with the Oak Ridge National Laboratory, Oak Ridge, TN 37831 USA (e-mail: f.wang@ieee.org).

R. Burgos is with the ABB U.S. Corporate Research Center, Raleigh, NC 27606 USA (e-mail: rburgos@ieee.org).

D. Boroyevich is with the Center for Power Electronics Systems, Virginia Tech, Blacksburg, VA 24061 USA (e-mail: dushan@vt.edu).

Color versions of one or more of the figures in this paper are available online at <http://ieeexplore.ieee.org>.

Digital Object Identifier 10.1109/TPEL.2009.2039004

The basic approach to limiting EMI emissions is the use of filters to attenuate the noise level to the frequency range specified in the standard. The design of these filters is very complex, and trial-and-error is often needed to achieve a filter that can meet the specifications. An inadequate filter design can result in poor performance, high cost, and a larger size than required. The last aspect is of utmost importance for high-power-density applications, since EMI filters usually account for as much as 30% of the total converter weight [2]. In consequence, reduction of EMI filter size has become a key design goal for power electronics equipment.

During the last decade, many papers have proposed procedures for designing EMI filter [3], [4]. A step-by-step method is used in [3] to obtain the required attenuation, corner frequency, and the filter parameters. Unfortunately, this method only fulfills the low-frequency (LF) requirement and suggests a trial-and-error process for high frequencies (HFs). The unpredictable behavior at HFs is mainly due to the parasitics of the filter components such as the CM choke or the coupling between components [5], as well as their interaction with the noise source. These HF effects are usually worse when the size is reduced and the components are close together.

Since there is no established method for designing a high-density filter, this paper starts with a baseline design following the procedure in [3]. The baseline design is used to understand the parasitics and grounding effects, and to identify the various possibilities for achieving a high-density filter. Guidelines are developed for the design and implementation of EMI filters, providing an insightful approach to filter size reduction while avoiding the use of common yet erroneous practices. These guidelines for improved EMI filter design are developed by organizing existing filter technologies, using new material technologies, and adopting an integrated magnetic core arrangement, which successfully achieves better high-density design than previous approaches [6], [7]. Experimental results are presented to verify the proposed methodology.

## II. DESCRIPTION OF SYSTEM AND COMMON EMI FILTER

The system used for study is a commercial motor drive used as a dc-fed inverter connected to a fan load via a 10 m shielded cable. The cable has three phase conductors, one ground conductor, and a shield. The inverter is configured at 2.5 kW, 300 V, and has a switching frequency of 12 kHz. The experimental setup and equivalent schematic representation of the setup is shown in Fig. 1(a) and (b).

Depending on the application, different standards might be required, necessitating different experimental setups, noise-level

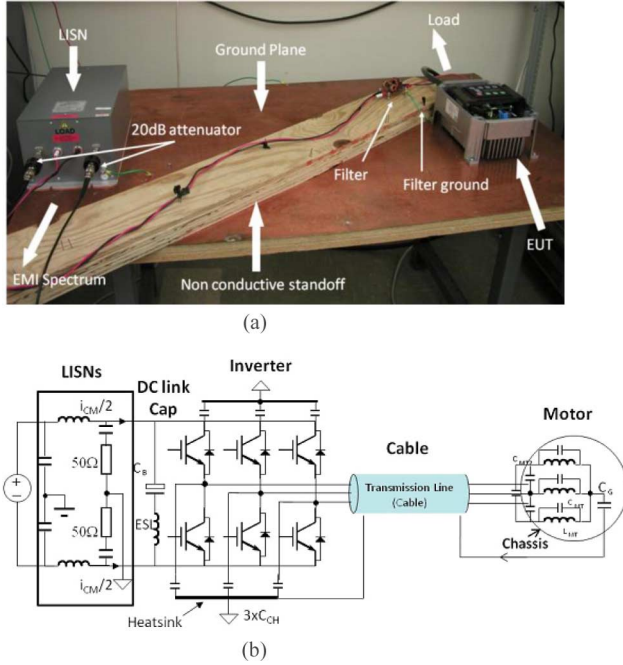


Fig. 1. DC-fed motor drive system under study. (a) Experimental setup and (b) schematics.

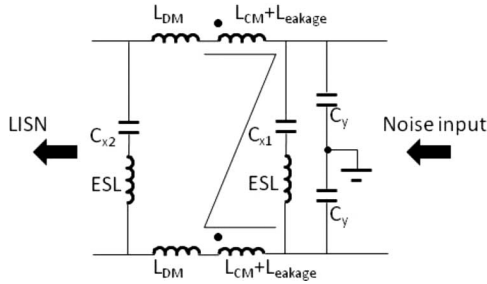


Fig. 2. Commonly used single-stage EMI filter.

requirements, and frequency ranges. Additionally, there may be some constraints on the maximum CM capacitance due to leakage current safety standards. This paper uses the section of Military Standard 461E that defines the EMI noise limit for frequencies from 10 kHz to 10 MHz [8].

Fig. 2 shows a single-stage EMI filter that is commonly used as a low-pass filter. This filter is placed between the dc-link capacitor and the line impedance stabilization network (LISN), which is required for specific measurement conditions. With the goal of reducing both CM and DM noise, the filter is composed of DM capacitors  $C_{X1}$  and  $C_{X2}$  and CM capacitor  $C_Y$  to bypass the noise with their low impedance, while the high-impedance CM choke  $L_{CM}$  blocks the EMI noise. The choke is usually made of a high-permeability core such as ferrite, and mainly reduces the CM noise; nevertheless, its leakage is used as DM inductance. The leakage can be approximated using (1), which is from [9]. The number of turns  $N$  and winding angle  $\theta$  are identified to be the main parameters.  $A_e$  is the effective cross-sectional area of the core in centimeters square, and  $l_e$  is the effective length of the core in centimeters.  $\mu_{DM\_effective}$  is the

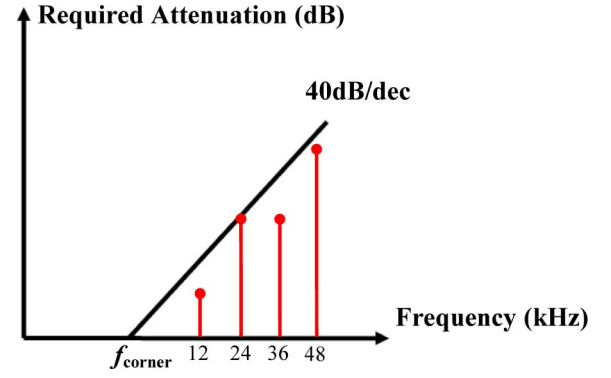


Fig. 3. Determining the required corner frequency based on theoretical attenuation.

effective relative permeability of the DM flux

$$L_{DM} = \mu_{DM\_effective} \frac{0.4\pi N^2 A_e}{l_e \sqrt{[(\theta/360) + (\sin(\theta/2)/\pi)]}} \times 10^{-8} \text{ (in Henry).} \quad (1)$$

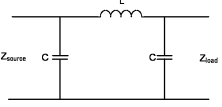
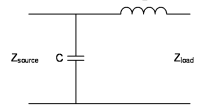
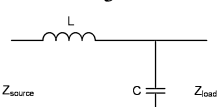
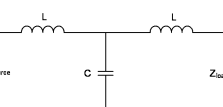
These factors are set during the design of the CM choke and cannot be easily changed without an impact on the CM choke size. For some applications, it is appropriate to add small DM inductors in series with the CM choke to increase the total DM inductance, thereby reducing the size of the DM capacitor. The structure presented at the end of this paper makes use of this idea by integrating these two cores into a single core, which has the desirable effect of significantly increasing the DM inductance. The total DM inductance increases threefold when compared to the leakage obtained by the CM choke alone.

The baseline filter is designed by determining the corner frequency required to attenuate LF CM and DM noise, and then determining the values of the filter components. The required attenuation for the highest switching harmonics is calculated by subtracting the standard limit for each mode from the original noise without a filter, then adding some margin, as shown in (2). The margin is needed since we are looking at each mode independently and not the total EMI noise. Finally, the theoretical attenuation slope is applied to the most stringent harmonic, and the corner frequency is obtained by (3). In (2) and (3),  $V$  stands for the noise signal (voltage) and  $f$  stands for corner frequency.

$$\begin{aligned} (V_{attenuation\_required})_{dB} &= (V_{original})_{dB} - (V_{standard})_{dB} + \text{margin} \\ f_{CM \text{ or } DM} &= \frac{f_{\text{for stringent harmonic}}}{10^{(V_{attenuation\_required})_{dB} / (\text{Filter's attenuation})_{dB/dec}}}. \end{aligned} \quad (2) \quad (3)$$

Fig. 3 is an example of CM noise, where a theoretical attenuation of 40 dB/dec is assumed due to the second-order low-pass filter. The corner frequency is determined by the second switching harmonics (24 kHz).

TABLE I  
SELECTION OF EMI FILTER TOPOLOGIES BASED ON NOISE SOURCE  
AND LOAD IMPEDANCES

$Z_{load}$ $Z_{source}$	High	Low
High	<p>1</p> 	<p>2</p> 
Low	<p>3</p> 	<p>4</p> 

### III. TOWARD A HIGH-DENSITY DESIGN

#### A. Topology Consideration

It is common to use one-stage or two-stage low-pass filter topologies, which allow for many possibilities by arranging the capacitors or inductors differently. The fundamental rule is to obtain the maximum impedance mismatch between the noise source and the filter. The basic topologies are given in Table I, and vary according to the source and load impedance of the filter.

The load impedance represented by the LISN is well known. The source impedance for CM noise is the parasitic capacitance in the motor, cable, and the motor drive. For the system under study, the measured parasitic capacitance is around 5 nF, most of which is contributed by the motor. The source impedance for the DM noise without the dc-link capacitor is usually very high at LFs because the impedance of the motor is very high. Therefore, the CM filter should use topology 2, and DM the filter should use topology 1 from Table I. For the CM filter, the CM capacitance should be much larger than parasitic capacitance so that the impedance mismatch rule is met. For the DM filter, the dc-link capacitor is part of the “ $\pi$ ”-type filter in topology “1.” The filter in Fig. 2 is an integration of CM and DM filters that has been tested and proven to provide the best attenuation and size reduction for both CM and DM noise.

The use of a multistage filter to further increase the attenuation and reduce the size of the filter could be useful in certain applications. However, when following the MIL461E standard specifications, this is not true for frequencies starting at 10 kHz, as the benefits of using more stages is very limited in this case and may not lead to a smaller filter size. This is because the required attenuation at LFs is relatively small. According to (3), the corner frequency of the EMI filter is very close to the frequency of the first noise peak regardless of the number of filter stages used. It is essential to remember that the constraints on the maximum CM capacitance due to the ground current safety standard still apply, and the total CM capacitance value will have to be split by the two stages. Consequently, the total CM

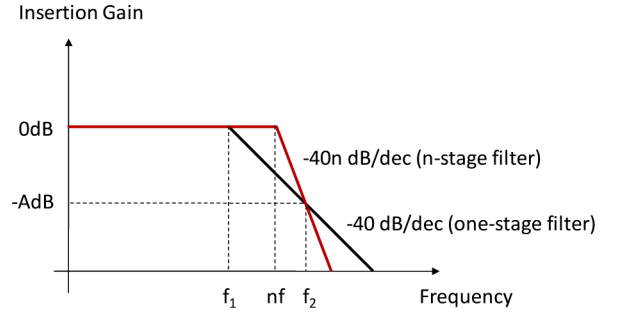


Fig. 4. Comparison of the insertion gains of one-stage and multistage EMI filters.

inductance of a multistage filter may be larger than the inductance of a one-stage filter. A similar principle applies to the DM filter. As a result, the final size of the multistage filter would be larger than that of a one-stage filter. On the other hand, if the required noise attenuation at LFs is high enough that the corner frequency is much smaller than the frequencies of the noise peaks, the multistage filter may be smaller than the one-stage filter. Fig. 4 demonstrates this principle.

In Fig. 4, it is assumed that the total inductance and capacitance of the one-stage filter are the same as they are in the multistage filters. It is also assumed that for the multistage filter, the inductance and capacitance on each stage are exactly the same. If an  $LC$  filter is used for each filter stage, the filter has an attenuation of  $-40$  dB/dec. The attenuation of an  $n$ -stage filter would be  $-40n$  dB/dec. If the corner frequency of a one-stage filter is  $f_1$ , the corner frequency of an  $n$ -stage filter would be equivalent to  $nf_1$ . In Fig. 4, at frequency  $f_2$ , the one-stage and the  $n$ -stage filters have the same attenuation of  $A$  dB. If the required attenuation is smaller than  $A$  dB, the one-stage filter would be more efficient, and may be smaller. If the required attenuation is higher than  $A$  dB, the multistage filter has the potential being smaller.

#### B. Grounding

Another important aspect to consider is the grounding of the filter, since CM noise propagates from the power circuit to ground. Consequently, the impedance of this grounding connection has a great impact on the filter performance. Some key parameters affecting this impedance are whether wire or copper foil is used, and the actual length of the connection. To study the effect of these factors, multiple measurements were conducted. The results show that the use of copper foils as ground interconnects helps reduce the CM noise in the system because they have smaller impedance [10]. The copper foils have a lower inductance than the same length of wire.

Figs. 5 and 6 depict the above phenomenon. The measurements were made with the same filter, only changing its type of connection to the ground plane. Specifically, the higher impedance trace corresponds to the case where a 30-cm-long wire is used to connect to ground, while for the lower impedance case, the filter was grounded simultaneously using a 15-cm-long wire and bolting it down directly to the motor drive heat sink. In the latter case, the two connections used provided two parallel



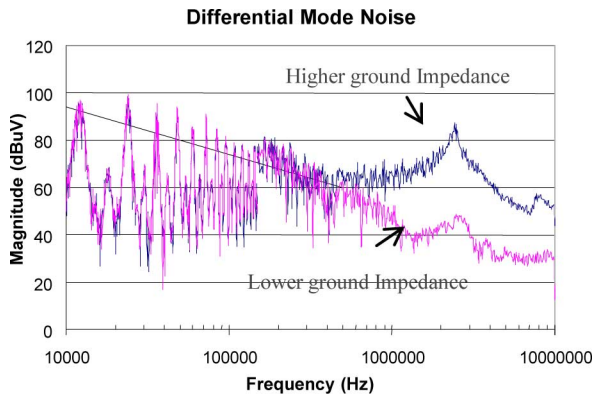


Fig. 5. Effects of grounding impedance on DM noise.

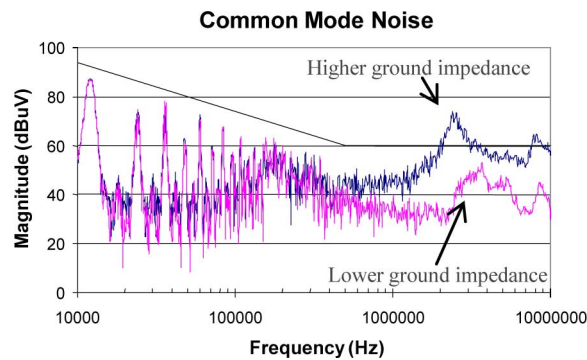


Fig. 6. Effects of grounding impedance on CM noise.

paths for the CM noise to flow, which is observed to effectively reduce the equivalent inductance by a factor of almost two. Finally, the type of grounding also affected the DM noise measurements, due to the structural asymmetry of the filter. It has been observed that when a “ $\pi$ ” filter topology is used for the DM noise, the asymmetry is greatly reduced and the impact of grounding on DM noise is limited.

Furthermore, for multistage filters, it is important to take into consideration the number of grounding points. Choosing an inadequate grounding method could alter the filter performance and easily result in a higher final EMI noise. This can be managed by using separate grounding points for each stage, which effectively prevents the LF stage from disturbing the HF stage. Fig. 7 shows this effect. It is worthwhile to note that the inductive couplings between different grounding paths should be minimized. A more detailed study on grounding is presented in [10], but the main point here is that an improper ground connection scheme can easily lead to an oversized filter design.

### C. CM Choke Size Optimization

In order to achieve a high-density EMI filter, the size of the DM capacitors and CM choke needs to be minimized. Many inductor designs are possible [11]; however, few methods focus on the total space utilization. Fig. 8 depicts the evolution of an EMI filter when its design is focused on size reduction.

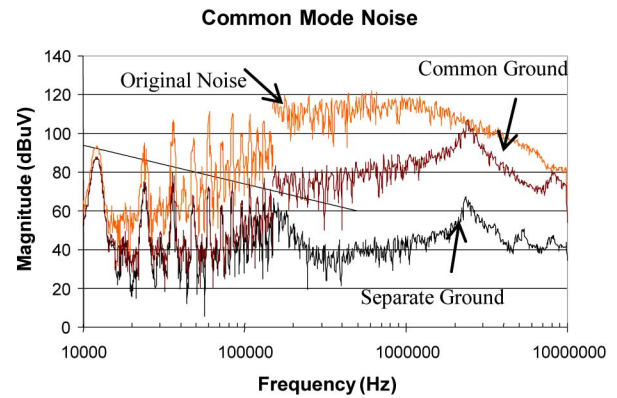


Fig. 7. Improving CM filter performance by using separate ground in a multistage filter.



Fig. 8. Filter size reduction. (Top) Baseline design; (middle) smaller CM choke with multilayer winding and increased current density; (bottom) higher current density, more turns per layer and with HF nanocrystalline core to increase HF noise attenuation.

The top filter is a baseline design that meets the MIL461E standard. The filter was designed for a 2-kW application with a dc voltage of 300 V. The size of the CM choke in this case is large. For the baseline design, the current density was set to 400 A/cm<sup>2</sup>, which is reasonably high per usual practice. However, as long as the thermal condition permits, the current density can be pushed higher. After multiple prototypes and thermal studies, it has been observed that the filter still works properly after doubling the current density, while its overall size is reduced, as shown on the bottom filter. The thermal image shown in Fig. 9 depicts the thermal condition of the bottom filter at steady state under rated operating conditions with an input current of 6.6 A. No extra cooling was used and the temperature reached steady state at around 80 °C, which is well below the maximum allowed temperature for the ferrite core and windings. Note also that the temperature rise is mainly due to the winding loss, since the core loss is typically small.

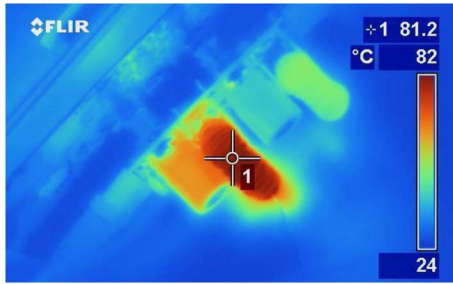


Fig. 9. Filter thermal image 30 min after running at 2 kW, 300 V dc, and 6.6 A.



Fig. 10. Size reduction of CM chokes after using multilayered winding and higher current density (see Table II).

TABLE II  
CM CHOKE'S PARAMETERS FOR FERRITE CORE

Parameters	Ferrite 1	Ferrite 2	Ferrite 3
Current Density (A/cm <sup>2</sup> )	≈400	≈600	≈800
Wire Gauge #	14	16	18
# of Turns per side	23	24	36
$L_{CM}$ (mH) @5kHz	3.1	3.7	4.6
Leakage (μH) @5kHz	36.1	30.3	53.7
EPC (pF)	11.8	30.7	51.6

Another optimization that can be pursued for these CM chokes is the winding method. As seen in Fig. 10, the winding area for ferrite 1 is quite empty, and hence, more turns could be applied. When designing the same inductance, the use of multilayer windings permits the use of much smaller cores, especially when thinner wire is used. At the same time, the use of multilayer windings changes the parasitics of the inductors, and hence, their behavior at HF. Specifically, the effective parallel capacitance (EPC), which is the parasitic capacitance of the inductor winding, increases significantly since the distance between each turn is smaller, making the EPC bigger. Nevertheless, a method such as that proposed in [12] could help to cancel out the EPC, achieving better performance at HF. However, the winding window and size reduction cannot be done arbitrarily; otherwise, the saturation of the core could become an issue. This is why the winding window of ferrite 3 in Fig. 10 is still significant due to the cross-sectional area required and the availability of commercial cores.

Table II summarizes the parameters of these three inductors; however, it should be noted that the cores, number of turns and wire gauges are different for each inductor. All parameters have been extracted with the impedance analyzer Agilent 4294 A.

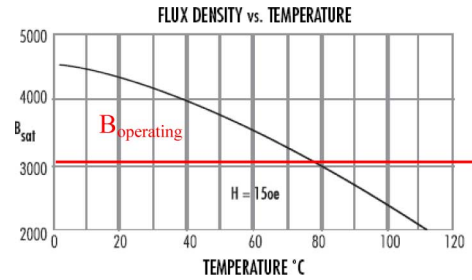


Fig. 11. Ferrite's saturation flux density as a function of temperature.

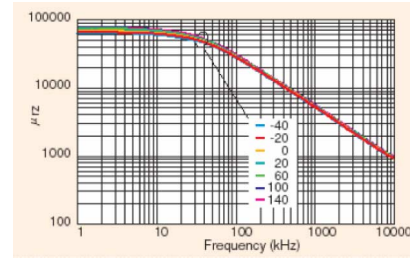


Fig. 12. Relative permeability of nanocrystalline material versus temperature (in degree Celsius) and frequency.

Increasing the current density and using multilayer windings are effective ways to reduce the size of the CM choke and the entire filter volume. As shown in Fig. 8, the total filter footprint is reduced nearly threefold. However, it is important to mention that these methods do have some drawbacks, such as a higher EPC and a higher operating temperature. The increase in temperature may be problematic for the application, and will affect the flux density saturation ( $B_{sat}$ ), which is a function of the temperature. Specifically, the  $B_{sat}$  of the ferrite core can become much lower at higher temperatures and lead to saturation due to the DM current; consequently, the impedance of the CM choke will be dramatically reduced and fail to meet the standard. To illustrate this fact, Fig. 11 shows the saturation flux density for ferrite as function of temperature. If the operating saturation point is set to 3000 G, or 0.3 T, and the temperature increases to above 80 °C, then the core could saturate since  $B_{sat} < B_{operating}$ .

A good way to avoid this unwanted performance is by using different magnetic materials, such as nanocrystalline cores, where the magnetic flux saturation is much higher [13] and the permeability does not change with respect to temperature. The next section compares these two technologies and determines under what conditions they are most suitable.

#### D. Magnetic Core Material

Nanocrystalline cores seem to be the most suitable material for CM chokes due to their high permeability, which is approximately three times higher than ferrite; higher saturation of 1.3 T compared to 0.4 T for most ferrite cores; and high Curie temperature of 570 °C. Additionally, as stated above, the permeability is much less sensitive to temperature. Therefore, the impedance permeability has the same characteristics at 140 °C as it does at 60 °C, as shown in Fig. 12. Finally, the behavior

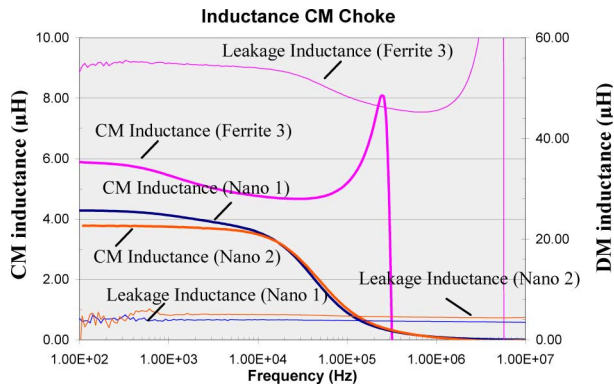


Fig. 13. CM inductance (thicker) and leakage inductance (thinner) for ferrite 3 (pink) and two nanocrystalline (orange and blue) cores with different sizes.

TABLE III  
CM CHOKE PARAMETERS FOR NANOCRYSTALLINE CORES

Parameters	Ferrite 3	Nano 1	Nano 2	Nano 3
Current Density ( $A/cm^2$ )	800	800	800	800
Wire Gauge #	18	18	18	18
# of Turns per side	36	11	14	24
$L_{CM}$ (mH) @5kHz	4.6	3.8	3.7	19.3
Leakage ( $\mu H$ ) @5kHz	53.7	4.1	5.0	18.3

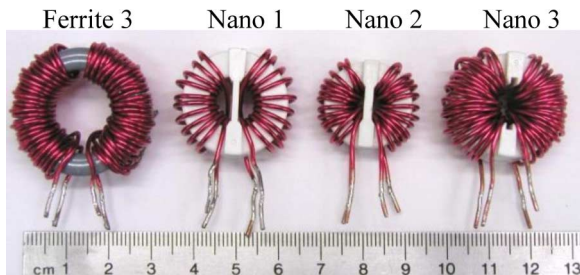


Fig. 14. Comparison of CM chokes using ferrite cores and nanocrystalline cores.

of nanocrystalline cores at HF is improved due to higher loss in this frequency range. However, some precautions need to be taken when designing the other parameters of the filter. First, since the permeability of nanocrystalline cores is much higher, the number of turns required to obtain the same inductance will be lower than using ferrite, which creates a much smaller leakage. The leakage of the core could be estimated, as in [9], where it is almost independent of core permeability for relative permeability ( $\mu_r$ ) higher than 5000. Consequently, the DM noise is greatly affected by this reduced leakage, especially if no other DM inductances are added in the circuit. This effect is shown in Fig. 13, where it can be easily observed that the initial leakage for the ferrite core used previously is around  $54 \mu H$ , while for the nanocrystalline core it is only around  $5 \mu H$ . As discussed above, this is due to the fact that the ferrite core has 36 turns, while the nanocrystalline only 11 turns. For reference, Table III shows the parameters of each choke, while Fig. 14 illustrates the relative size between inductors.

Another interesting point to note is the behavior of the nanocrystalline core at the midrange frequencies (between 10

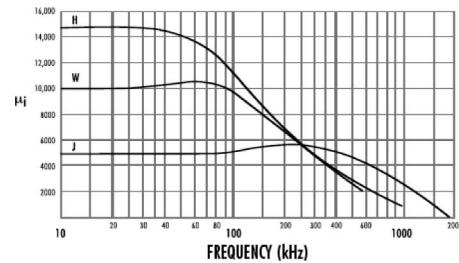


Fig. 15. Relative permeability of ferrite core versus frequency.

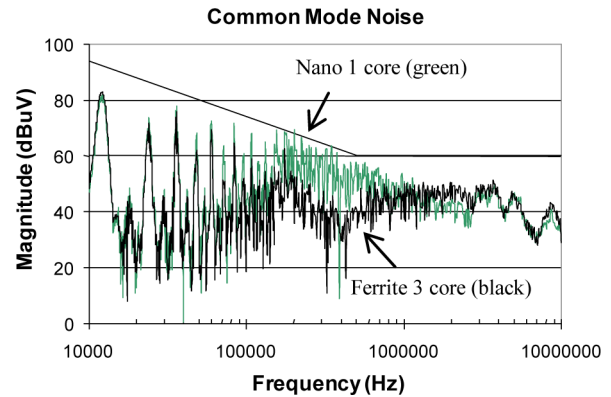


Fig. 16. Comparison of measured CM noise with ferrite and nanocrystalline cores.

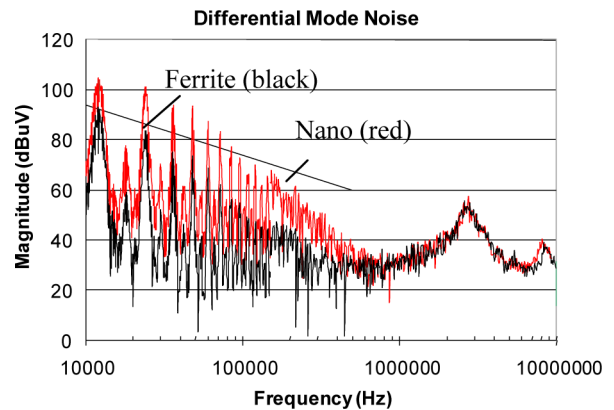


Fig. 17. Comparison of measured DM noise with ferrite and nanocrystalline cores.

and 250 kHz) where its permeability drops much faster than ferrite. The permeability–frequency curves for nanocrystalline materials and ferrite are shown in Figs. 12 and 15, while the corresponding measurement results are shown in Fig. 13.

The behaviors predicted theoretically are easily identified in the power tests in Figs. 16 and 17, where the CM noise is higher in the midrange frequencies, while the DM noise is greatly increased at LF due to the small leakage. It is important to mention that the filter used with ferrite 3, represented at the bottom of Fig. 8, combines a small HF nanocrystalline core to attenuate the HF noise. For the measurements with the Nano 1, HF core have been removed since the main choke has better performance at HF because the overall size is reduced.





Fig. 18. New integrated CM and DM inductor.

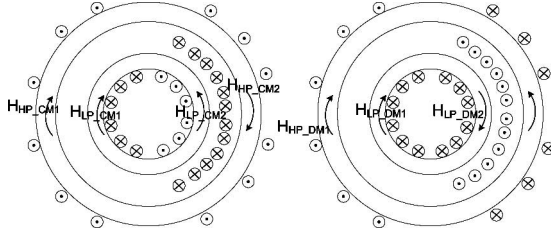


Fig. 19. Magnetic field intensity for CM current (left) and DM current (right) in the new structure.

Many more tests were conducted with nanocrystalline cores to compensate its drawbacks. A possible solution for overcoming these drawbacks is to use multilayer windings to increase the number of turns, and therefore, augment the leakage and CM inductance, as shown with the Nano 3 core in Fig. 14.

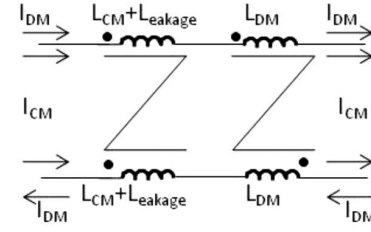
The use of nanocrystalline material depends on the application, and tradeoffs between other technologies should be studied on a case-by-case basis. Its size reduction and behavior at HF are its major advantages.

#### E. Integrated CM and DM Inductor

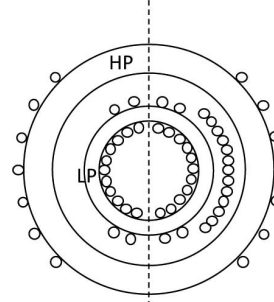
The two main obstacles to designing a small EMI filter are the CM choke and the DM capacitor, which can be of significant size. To reduce the capacitor size, advanced technologies such as low-profile planar ceramic capacitors could be employed. Reducing the capacitance value through the proper increase of DM inductances is also an effective approach, which can be achieved using a multistage DM filter or increasing the filter's DM inductance. Since the leakage from the CM choke cannot be increased arbitrarily, it is common practice to add DM inductances in series with the CM choke at the expense of an increased total volume of the filter.

This paper adopts a new integrated inductor configuration to minimize the size of the EMI filter, taking advantage of the readily available window area of the CM choke and placing a low-permeability core within the choke structure. Specifically, a Kool Mu core is used in this case. It has the capability to increase the total leakage of the choke or DM inductance. Fig. 18 shows the proposed integrated inductor. The object is to use the same winding for both cores, as proposed in [7], but to reduce the size by using a single low-permeability core.

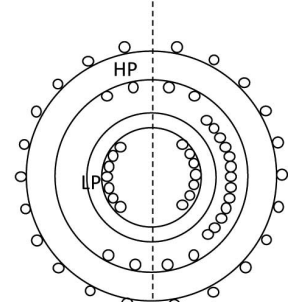
Since only one DM core is used in the proposed filter, the winding method had to be changed, interweaving the winding, as shown in Figs. 18 and 19. On one side, both cores are wound



(a)



(b)



(c)

Fig. 20. Integrated choke. (a) Equivalent structure for the integrated choke, (b) DM inductor has more turns than CM inductor, and (c) CM inductor has more turns than DM inductor.

together, while for the other side, they are counterwound so that the wire is wound in a shape 8. Fig. 19 shows the direction of each magnetic field for the CM and DM current of each core. The cores are denoted HP for high permeability, which is the ferrite core, and LP for low permeability, which is the Kool Mu core.

For the high-permeability core, it follows that

$$\sum \phi_{CM} = \phi_{CM1} + \phi_{CM2} = 2\phi_{CM}, \quad \text{with } \phi_{CM1} = \phi_{CM2} \quad (4)$$

$$\sum \phi_{DM} = \phi_{DM1} - \phi_{DM2} = 0, \quad \text{with } \phi_{DM1} = \phi_{DM2}. \quad (5)$$

And for the low-permeability core, we have

$$\sum \phi_{CM} = \phi_{CM1} - \phi_{CM2} = 0, \quad \text{with } \phi_{CM1} = \phi_{CM2} \quad (6)$$

$$\sum \phi_{DM} = \phi_{DM1} + \phi_{DM2} = 2\phi_{DM}, \quad \text{with } \phi_{DM1} = \phi_{DM2}. \quad (7)$$

In the equations above,  $\phi_{CM}$  is the total CM magnetic flux in the core,  $\phi_{CM1}$  and  $\phi_{CM2}$  are the CM magnetic flux generated by each of the two windings,  $\phi_{DM}$  is the total DM magnetic flux in the core, and  $\phi_{DM1}$  and  $\phi_{DM2}$  are the DM magnetic flux generated by each of the two windings. Equations (4)–(7) describe the magnetic field of each core, and show that the high-permeability core mainly contributes to CM inductance, while the low-permeability core creates DM inductance. The equivalent circuit for the structure is shown in Fig. 20(a). Fig. 21 presents a comparison of the small-signal response of the integrated structure and the same core with the same number of turns but without using the low-permeability core. The CM

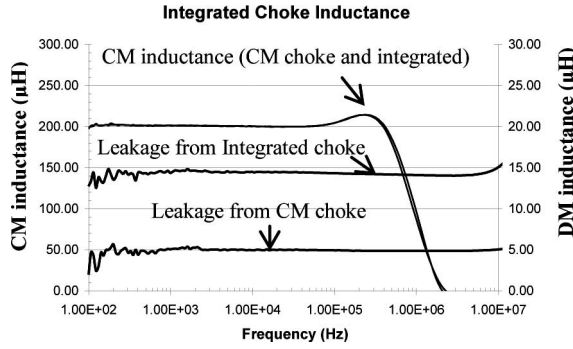


Fig. 21. Comparison of CM inductance and leakage inductance between CM choke and integrated choke.

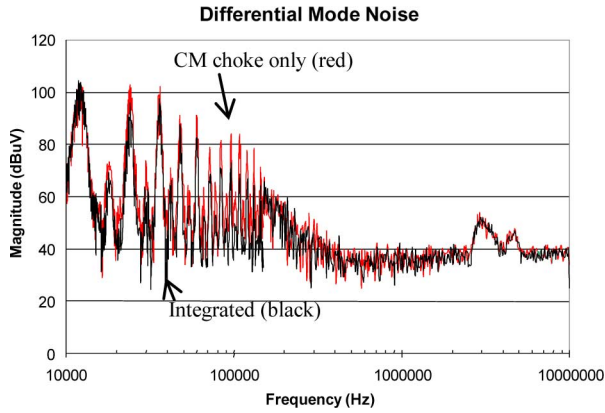


Fig. 22. Comparison of measured DM noise between filters with CM choke and integrated choke.

inductance is almost the same, while it is obvious that the DM inductance has increased by at least three times compared to using the CM choke only.

The large-signal tests conducted are shown in Fig. 22, which depicts the DM attenuation attained. The CM noise is not shown since both cores present the same noise impact. The integrated choke was designed to have a 200  $\mu\text{H}$  CM inductance and 5  $\mu\text{H}$  leakage inductance. It is clear that between 20 and 150 kHz the integrated choke has better performance than the regular choke, with 8–18 dB more attenuation. The same technique has also been used successfully with a nanocrystalline core to compensate for the small leakage.

When the DM and CM inductors have different numbers of turns, the structures in Fig. 20(b) and (c) can be used. Fig. 20(b) is the structure when the DM inductor (inner core) has more turns than the CM inductor. Fig. 20(c) shows the structure when the CM inductor (outer core) has more turns than the DM inductor. Because the integrated inductor structure and the multilayer winding solution discussed in Section III-C cannot be used at the same time, an evaluation is usually necessary before making a structure selection. This evaluation should follow the flowchart in Fig. 23. The integrated inductor structure usually has a larger DM inductance than the multilayer winding structure due to the existence of a DM core, so the filter with this structure is more suitable for a power electronics system with high DM noise. When the DM noise is low enough such that a multilayer

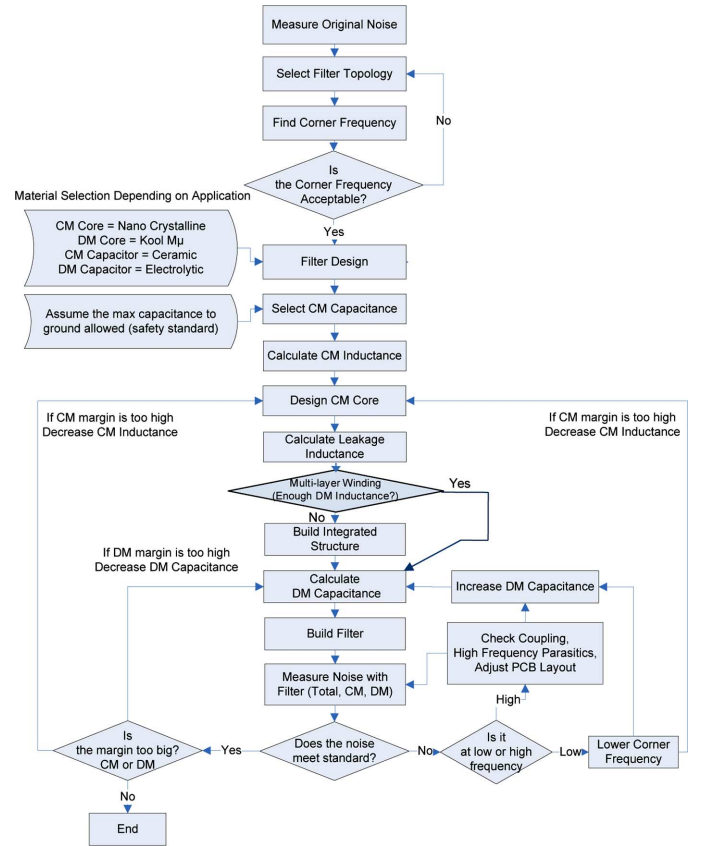


Fig. 23. Flowchart for the design procedure of an EMI filter.

winding structure can provide enough DM inductance for DM noise attenuation, the multilayer winding structure would be a better choice.

#### F. Summary

To minimize the total size of EMI filter, it is necessary to choose the correct filter components and use them close to their electrical, thermal, and mechanical limits. However, knowing the filter application and environment is also very important during the design stage, since the operating conditions, temperature and adherence to standards impact the design process. The best filter topology for one application may not be the best for other applications.

The flowchart in Fig. 23 illustrates a procedure for designing a high-density EMI filter for the previous application.

#### IV. CONCLUSION

This paper presents several aspects important for the design of high-density EMI filters for dc-fed motor drives. Grounding issues, circuit topologies, and a series of methods to reduce the overall filter size are presented. These methods include the use of multilayer windings to maximize the window area of the core, and the use of advanced magnetic materials such as a nanocrystalline core. Furthermore, a new inductor structure is proposed that integrates both CM and DM inductances, taking advantage of the CM choke available window area. This novel integrated



design is verified through its small-signal and large-signal response, and performs well across the frequency spectrum while achieving the desired size reduction.

## REFERENCES

- [1] S. Wang, F. Lee, and W. Odendaal, "Characterization, evaluation, and design of noise separator for conducted EMI noise diagnosis," *IEEE Trans. Power Electron.*, vol. 20, no. 4, pp. 974–982, Jul. 2005.
- [2] S. D. Round, P. Karutz, M. L. Heldwein, and J. W. Kolar, "Towards a 30 kW/liter, three-phase unity power factor rectifier," in *Proc. PCC2007*, Apr., pp. 1251–1259.
- [3] F. Shih, D. Chen, Y. Wu, and Y. Chen, "A procedure for designing EMI filters for AC line applications," *IEEE Trans. Power Electron.*, vol. 11, no. 1, pp. 170–181, Jan. 1996.
- [4] K. Gulez, N. Mutoh, F. Harashima, and K. Ohnishi, "An approximation to EMI noise problem to design an appropriate EMI filter for induction motor control systems," in *Proc. SICE2001*, Jul., pp. 6–11.
- [5] S. Wang, F. C. Lee, D. Y. Chen, and W. G. Odendaal, "Effects of parasitic parameters on EMI filter performance," *IEEE Trans. Power Electron.*, vol. 19, no. 3, pp. 869–277, May 2004.
- [6] P. Boonma, V. Tarateeraseth, and W. Khan-ngern, "A new technique of integrated EMI inductor using optimizing inductor volume approach," in *Proc. IPEC2005*, pp. 1–5.
- [7] L. Nan and Y. Yugang, "A common mode and differential mode integrated EMI filter," in *Proc. IEEE Trans. Power Electron. Motion Control Conf. (IPEMC 2006)*, Aug., vol. 1, pp. 1–5.
- [8] Requirements for the control of electromagnetic interference characteristics of subsystems and equipment, Military Standard 461E, Aug. 1999.
- [9] M. Nave, "On modeling the common mode inductor," in *Proc. IEEE Trans. Electromagn. Compat.*, Aug. 1991, pp. 452–457.
- [10] S. Wang, Y. Maillet, F. Wang, and D. Boroyevitch, "Investigating EMI filter's grounding in power electronics system," in *Proc. PESC2008*, pp. 4375–4380.
- [11] R. West, "Common mode inductors for EMI filters require careful attention to core material selection," *PCIM Mag.*, Jul. 1995.
- [12] S. Wang, F. Lee, and J. Wyk, "Inductor winding capacitance cancellation using mutual capacitance concept for noise reduction application," *IEEE Trans. Electromagn. Compat.*, vol. 48, no. 2, pp. 311–318, May 2006.
- [13] *FINEMET CM Choke Cores, Technical Bulletin*, Metglas, Conway, SC, 2004, p. 1.
- [14] Q. Liu, S. Wang, F. Wang, C. Baisden, and D. Boroyevich, "EMI suppression in voltage source converters by utilizing DC-link decoupling capacitors," *IEEE Trans. Power Electron.*, vol. 22, no. 4, pp. 1417–1428, Jul. 2007.
- [15] P. Kong, S. Wang, and F. C. Lee, "Common mode EMI noise suppression for bridgeless PFC converters," *IEEE Trans. Power Electron.*, vol. 23, no. 1, pp. 291–297, Jan. 2008.
- [16] P. Kong, S. Wang, C. Wang, and F. C. Lee, "Common-mode EMI study and reduction technique for the interleaved multichannel PFC converter," *IEEE Trans. Power Electron.*, vol. 23, no. 5, pp. 2576–2584, Sep. 2008.
- [17] H. Akagi and T. Shimizu, "Attenuation of conducted EMI emissions from an inverter-driven motor," *IEEE Trans. Power Electron.*, vol. 23, no. 1, pp. 282–290, Jan. 2008.
- [18] S. Wang, F. C. Lee, and J. D. van Wyk, "A study of integration of parasitic cancellation techniques for EMI filter design with discrete components," *IEEE Trans. Power Electron.*, vol. 23, no. 6, pp. 3094–3102, Nov. 2008.



**Yoann Maillet** received the B.S. degree in electrical engineering from Virginia Polytechnic Institute and State University (Virginia Tech), Blacksburg, in 2006, and the M.S. degree from the Center for Power Electronics Systems (CPES), Virginia Tech, in 2008.

Since 2008, he has been an Electrical Engineer at Conver Team, Inc., Pittsburg, PA. His current research interests include passive electromagnetic interference (EMI) filter design, integrated EMI choke for common-mode (CM) and differential-mode (DM) suppression.



**Rixin Lai** (S'07–M'10) received the B.S. and M.S. degrees in electrical engineering from Tsinghua University, Beijing, China, in 2002 and 2005, respectively, and the Ph.D. degree from the Center for Power Electronics Systems (CPES), Virginia Polytechnic Institute and State University (Virginia Tech), Blacksburg, in 2008.

In 2009, he joined the Electronic Power Conversion Laboratory, Global Research Center of General Electric Company, Niskayuna, NY. His current research interests include the passive filter design, electromagnetic interference (EMI) technology, modeling and control of three-phase converters, and high-power-density converter development.



**Shuo Wang** (S'03–M'06–SM'07) received the B.S.E.E. degree from the Southwest Jiaotong University, Chengdu, China, in 1994, the M.S.E.E. degree from Zhejiang University, Hangzhou, China, in 1997, and the Ph.D. degree from the Center for Power Electronics Systems (CPES), Virginia Polytechnic Institute and State University (Virginia Tech), Blacksburg, in 2005.

He has been with the Electrical Power Systems, GE Aviation Systems, Vandalia, OH, since 2009. He was a Research Assistant Professor at the Center for

Power Electronics Systems, Virginia Tech, from 2005 to 2009. He holds four U.S. patents and has another two pending. He has authored or coauthored more than 70 academic papers in the IEEE Transactions and the IEEE conferences. His current research interests include EMI/EMC in power electronics systems, high-density-power conversion, three-phase power conversion and inversion, motor drive, generator control, and power systems.

Dr. Wang received the 2005 Best Transaction Paper Award from the IEEE Transactions on Power Electronics and the William M. Portnoy Award for the best paper published in the IEEE IAS Annual Conference in 2004. He is an Associate Editor for the IEEE TRANSACTIONS ON INDUSTRY APPLICATIONS.



**Fei (Fred) Wang** (S'85–M'91–SM'99–F'10) received the B.S. degree from Xi'an Jiaotong University, Xi'an, China, and the M.S. and Ph.D. degrees from the University of Southern California, Los Angeles, in 1982, 1985, and 1990, respectively, all in electrical engineering.

From 1990 to 1992, he was a Research Scientist in the Electric Power Laboratory, University of Southern California. In 1992, he joined the GE Power Systems Engineering Department, Schenectady, NY, as an Application Engineer. From 1994 to 2000, he was

a Senior Product Development Engineer with GE Industrial Systems, Salem, VA. From 2000 to 2001, he was the Manager of Electronic and Photonic Systems Technology Laboratory, GE Global Research Center, Schenectady, and Shanghai, China. In 2001, he joined the Center for Power Electronics Systems (CPES), Virginia Polytechnic Institute and State University (Virginia Tech), Blacksburg, as a Research Associate Professor and became an Associate Professor in 2004. During 2003, he was also the CPES Technical Director. In 2009, he joined The University of Tennessee, Knoxville and Oak Ridge National Lab, Knoxville, TN, as Condra Chair Professor of power electronics. His current research interests include power electronics, power systems, controls, electric machines, and motor drives.



**Rolando Burgos** (S'96–M'03) received the B.S. degree in electronics engineering, the Electronics Engineering Professional degree, and the M.S. and Ph.D. degrees in electrical engineering from the University of Concepcion, Chile, in 1995, 1997, 1999, and 2002, respectively.

In 2002, he joined the Center for Power Electronics Systems (CPES), Virginia Polytechnic Institute and State University (Virginia Tech), Blacksburg, as Postdoctoral Fellow, becoming a Research Scientist in 2003 and a Research Assistant Professor in 2005.

In 2009 he joined the ABB U.S. Corporate Research Center, Raleigh, NC, where he is currently a Power Electronics Consulting R&D Engineer. His research interests include multiphase and multilevel power conversion, stability of ac and dc power electronics systems, hierarchical modeling, control theory, and the synthesis of power electronics conversion systems.

Dr. Burgos is member of the IEEE Power Electronics, Industrial Electronics, Industry Applications and Power Engineering Societies, and is currently the Secretary of the Committee on Simulation, Modeling and Control of the Power Electronics Society.



**Dushan Boroyevich** (S'81–M'86–SM'03–F'06) received the Dipl.Ing. degree from the University of Belgrade, Belgrade, Serbia, in 1976, the M.S. degree from the University of Novi Sad, Novi Sad, Serbia, in 1982, and the Ph.D. degree from Virginia Polytechnic Institute and State University (Virginia Tech), Blacksburg, in 1986.

From 1986 to 1990, he was an Assistant Professor and the Director of the Power and Industrial Electronics Research Program in the Institute for Power and Electronic Engineering, University of Novi Sad, and later, the Acting Head of the institute. He then joined the Bradley Department of Electrical and Computer Engineering, Virginia Tech, as an Associate Professor, where he is currently the American Electric Power Professor in the department and the Codirector of the Center for Power Electronics Systems (CPES).

Dr. Boroyevich is a recipient of the IEEE William E. Newell Power Electronics Technical Field Award.

His current research interests include multiphase power conversion, electronic power distribution systems, power electronics systems modeling and control, and multidisciplinary design optimization.